Measurements of Acceleration on Delta GEM Boosters and Road Tests of GPS Position Sensing

25 July 2000

Prepared by

S. T. AMIMOTO, D. J. CHANG, E. W. FOURNIER,
and E. M. YOHNSEE
Space Materials Laboratory
Laboratory Operations

Prepared for

SPACE AND MISSILE SYSTEMS CENTER
AIR FORCE MATERIEL COMMAND
2430 E. El Segundo Boulevard
Los Angeles Air Force Base, CA 90245

Space Systems Group

20000905 050

**THE AEROSPACE
CORPORATION**
El Segundo, California

DTIC QUALITY INSPECTED 4
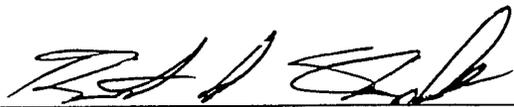
1 Lt Brent A. Shepherd
SMC/CLM

REPORT DOCUMENTATION PAGE

Form Approved
OMB No. 0704-0188

1. AGENCY USE ONLY (*Leave blank*)	2. REPORT DATE 25 July 2000	3. REPORT TYPE AND DATES COVERED

4. TITLE AND SUBTITLE Measurements of Acceleration on Delta GEM Boosters and Road Tests of GPS Position Sensing	5. FUNDING NUMBERS F04701-93-C-0094
6. AUTHOR(S) S. T. Amimoto, D. J. Chang, E. W. Fournier, and E. M. Yohnsee	

7. PERFORMING ORGANIZATION NAME(S) AND ADDRESS(ES) The Aerospace Corporation Laboratory Operations El Segundo, CA 90245-4691	8. PERFORMING ORGANIZATION REPORT NUMBER TR-2000(1494)-3

9. SPONSORING/MONITORING AGENCY NAME(S) AND ADDRESS(ES) Space and Missile Systems Center Air Force Materiel Command 2430 E. El Segundo Boulevard Los Angeles Air Force Base, CA 90245	10. SPONSORING/MONITORING AGENCY REPORT NUMBER SMC-TR-00-27

11. SUPPLEMENTARY NOTES

12a. DISTRIBUTION/AVAILABILITY STATEMENT Approved for public release; distribution unlimited	12b. DISTRIBUTION CODE

13. ABSTRACT (*Maximum 200 words*)

The results of an effort to localize the position of impact on a Delta graphite epoxy motor (GEM) case using accelerometers are reported. Acceleration from impacts produced by a hammer on an empty case was easily sensed using 50-g accelerometers. When the motor case is filled with inert propellant, the magnitude of the acceleration is reduced and damped out rapidly, making detection at longer distances over 2 m more difficult unless more sensitive accelerometers are used.

A method to localize or triangulate an impact location was developed and tested using acceleration data. It was necessary to filter the data to reduce its bandwidth to reduce dispersion effects that affect the velocities of the disturbances being sensed. The disturbances were shown to originate from structural deformations.

Results from road tests to sense the locations of a GEM motor using GPS are reported. The motor was driven over select roads at Edwards AFB.

This effort was part of a larger effort to monitor the health of GEM motor cases at Edwards. Further details of tests at Edwards AFB are described in "Health monitoring for Graphite/Expoxy Motor Cases," ed. by R. Welle, Aerospace Technical Report, TR-2000(1222)-1

14. SUBJECT TERMS Graphite epoxy solid rocket motors, Health monitoring, Impact triangularization, Accelerometers		15. NUMBER OF PAGES 23
		16. PRICE CODE

17. SECURITY CLASSIFICATION OF REPORT UNCLASSIFIED	18. SECURITY CLASSIFICATION OF THIS PAGE UNCLASSIFIED	19. SECURITY CLASSIFICATION OF ABSTRACT UNCLASSIFIED	20. LIMITATION OF ABSTRACT

Contents

Figures

Tables

Preceding Page's Blank

1. Introduction

This report documents the efforts using accelerometers as a means to monitor the status of the Delta II GEM motor casings. The vibrational and wave propagation characteristics of the empty booster case at Aerospace and the inert-filled booster at AFRL/Edwards were measured using a suite of accelerometers. The sensor suite consisted of five physically distinct sensors. Two sensors used dual, longitudinal- and latitudinal-sensing accelerometers. The remaining three were single-axis accelerometers oriented in the longitudinal direction. The objectives of this study were to develop a methodology to measure wave speeds on the cylindrical casing and to triangulate impact locations over large distances. Data were also taken for impact tests and for the road tests, but are inconclusive due to the use of insensitive accelerometers.

2. Experimental Methods

Wave speed data were acquired using a set of two-axis 50-g accelerometers oriented in the circumferential and longitudinal booster directions. The accelerometers were first placed along the top azimuth of the empty, horizontally positioned motor case located in Bldg. 130, SMC/LAAFB. The locations of the longitudinally aligned accelerometers were (50, 0), (100, 0), (150, 0), and (200, 0). The sensor locations for the circumferentially aligned accelerometers were (50, 0), (50, 35), (50, 70), and (50, 105). The dimensional unit is cm. The axes of the coordinate system are defined as x and y, where x is measured along the top from the north end (away from the "exhaust end") of the case, and the circumferential y axis is measured with respect to its origin at the x axis, which runs along the top of the cylindrical shell. The north end of the case is located at $x = -50$, and, therefore, the origin of the x axis is located 50 cm south from the north end. The circumferential direction has a positive sign for locations accessible from the west of the cylinder.

The data from the accelerometers were recorded using two types of instrumentation systems. For the preliminary effort at Aerospace on a segment of an empty booster case, a Tektronix digitizing oscilloscope, model TDS 540A, was used to digitize data at a rate of 250 kHz. Later data and data taken at Edwards AFB on the inert-filled booster were recorded using a Hitachi 166 MHz laptop with a National Instruments digitizing, PCMCIA card, model DAT-1200. For the impact tests to the inert-filled booster, AC power was used to power the instruments. For the road tests, however, a 12-V car battery with a DC-to-AC power converter was used to power the system. The Tektronix oscilloscope had only 4 channels, whereas the laptop based system had 8 channels. Data from the oscilloscope required conversion from binary to ASCI format prior to data analysis. Data were analyzed using IGOR software available from Wavemetrics.

The accelerometers used in the sensors were the model 250, ± 50 g from Analog Devices. In retrospect, the 5-g sensors should have been used for increased sensitivity. For tap testing performed with the empty booster at Aerospace, these were adequate. However, for tests at AFRL, they were inadequate due to the low response and the high damping experienced with the inert booster. The 3 dB response bandwidth (single pole) is 1.2 kHz. The booster shell was tapped using either a hard plastic impact hammer, a rubber mallet, or a wooden stick.

A switching filter was used to provide low-pass filtering as an anti-aliasing filter. An 8th-order elliptic, switched-capacitor filter (MAX7400CPA from Maxim) was selected. The signal-to-noise ratios for these filters are quite good, better than –60 dB over a 0.5 to 5.0 V input. However, below 0.1 V, the signal-to-noise ratio drops precipitously due to clock-noise leakage. Performance will be poor if signal levels are low or if signals vary over a high dynamic range. Signals for the impact test and road tests were generally near 1 g or less (38 mV for a ± 50 g accelerometer) and are sufficiently low that the signal-to-noise ratio would be poor. Use of a more sensitive accelerometer such as the ADL 105, a ± 5-g full-scale accelerometer would provide more than adequate signals for peak acceleration events.

For generating the wave-induced acceleration data, a rubber hammer with a sensor was used to impact the motor surface at predetermined locations along the line (longitudinal or circumferential) on which the accelerometers were mounted for each set of accelerometer arrangements. The rubber head of the hammer is approximately 4 in. long by 2.5 in. in diameter. The objective was to record the wave arrival time at each accelerometer from each impact. The impact locations for the longitudinal wave speed calculations were (–45, 0), (5, 0), (55, 0), and (105, 0). The impact locations for the circumferential wave speed calculations were (50, 0), (50 35), (50, –50), and (50, –100).

3. Data Analysis

The wave speeds were measured in the two principal directions, the longitudinal and circumferential. The wave speeds in any other direction can be determined using Eq. (1). It should be noted that the phase of the wave may vary in directions between the two principal directions, as observed by Olofsson.[1] The motor case is a shell composite structure, and there are two types of associated speeds. One is associated with the fiber material modulus and its density. For example, the longitudinal wave speed V_L of graphite fibers is $(E/\rho)^{1/2}$. This longitudinal wave speed associated with Young's modulus of the graphite fiber is very high, over 10 km/s. This wave can be observed as a disturbance arriving promptly, and no transit time information can be obtained. This wave was observed only when the edge of the cylindrical shell was tapped. The other type of wave is the structure response-induced wave whose frequency depends on the structural design and boundary conditions. The waves associated with the structural/elliptical deformation response of the tube were recorded when excited by taps normal to the exterior cylinder surface of the composite shells, and the resulting waveforms were used to determine their speeds.

Since the solid rocket motor case material, made of graphite/epoxy composite using a filament winding technique with a symmetric lay-up, has macroscopic orthotropic material properties, the wave speed for the composite is directionally dependent. Because of the orthotropy, it is expected that the deformation wave speed on the longitudinal-circumferential plane will take an elliptic form, i.e.,

$$V^2(\theta) = [V_x\cos(\theta)]^2 + [V_y\sin(\theta)]^2, \tag{1}$$

where θ is the angle between the longitudinal direction and the direction of interest. This equation is a phenomenological description of the propagating wavefront. It is also applicable to a propagating deformation wave in a flat plate. For isotropic[2,3] and orthotropic plates,[4] the Kirchhoff plate equations were shown to be a good model for the deformations. Kirchhoff models, in general, are precise solutions to the deformation of the surface as a function of time. They show that the wave speeds exhibit dispersion effects, whereby the wave speeds are a function of frequency. Yet, we may reconcile this difference between Eq (1), which assumes constant speed, and the Kirchhoff equations by restricting the wave speed to a narrow frequency regime whereby the speed is constant. Along the circumferential and longitudinal directions of a composite tube, the position of the wave was shown to be linear with time.[1] Agreement of the data with the modeling results for a cylindrical tube using a finite-element code was good in the circumferential direction for position and speed. In the longitudinal direction, agreement was good for the speed and fair for position, but, in all cases, position was linear with time. Simple plate models for the wavefront such as Eq (1) appear to be applicable to tubes. Hence, measured speeds on the rocket motor could be related to the waveforms observed by accelerometers and strain gauges. Accelerometer data could be analyzed for its frequency content, and a distance could be calculated based on the dispersion characteristics of the traveling waves that constitute the tube dynamics. Eq (1) was adopted under the assumption of elliptical waves for a plate and the decomposition of velocity for the two principle directions.

When the recorded wave data were analyzed, it was found that the wave arrival time, based on the visual inspection criteria of peak amplitude, did not provide consistent values. Upon a careful evaluation, it was determined that the impact generated a wide range of frequencies whose speeds varied considerably. Because of this, the calculated apparemt wave speed depended on the location that was impacted and on the object used to tap the empty shell. When the accelerometer was located at a distance greater than 100 cm from the impact, much of the high-frequency component of the waves was attenuated, and, therefore, the recorded wave arrival times at different accelerometers did not correspond to the same frequency or the same frequency range. The calculated wave speeds varied by as much as a factor of 2 from one dataset to another.

Assuming that the source of the discrepancy was due to dispersion or frequency dependent speeds, it was decided to choose a specific frequency range common to all the datasets. The filtering procedure is important in eliminating the high-frequency components, which have higher speeds, as shown in solutions to the Kirchoff equation. These high frequencies are only present for sensors close to the impact site since the high frequencies are attenuated rapidly with distance. Fourier spectrum analyses to produce power spectrum densities (PSD) were performed for all the waves. A frequency range between 500 and 1000 Hz was selected. The wave-time history within the selected frequency band was analyzed by first performing a Fourier transform, eliminating the contribution outside the frequency band, and then performing an inverse Fourier transform. This filtering procedure gave a longitudinal wave speed of 268 m/s with a standard deviation of 38 m/s, and a circumferential wave speed of 419 m/s with a standard deviation of 31 m/s. Figures 1 and 2 show typical linear fits of distance vs. arrival times for the filtered waves. Speeds were also measured by Olofsson[1] who used a laser holography method on small graphite tubes. He observed speeds of 400 and 500 m/s in the longitudinal and circumferential directions, respectively.

Impact data using a calibrated impactor with a 5/8-in. tup and a 30-lb proof mass produced impact histories with frequency content below 200 Hz but little above 200 Hz. Hence, the speeds measured and reported just previously are not valid for location of impacts by the calibrated impactor using the 5/8-in. tup on a 30-lb proof mass. For this reason, this mass was subsequently changed to a 10-lb proof mass for the tests performed at Edwards on the inert-filled booster to increase the frequency content of the vibrational waveforms.

Additional data was taken using the rubber hammer described earlier as an impact source. This data has lower frequency content than the dataset taken just prior to the impactor data, which used a plastic tipped hammer. Speeds from this dataset have not yet been analyzed. For this study, sensors and their locations were as shown in Table 1.

The impact locations for the rubber mallet were (185,0), (130,0), (80,0), (230,0), (50,80), (90,70), (180,70), (180,105), (180,35), (130,35), (130,70), (130,105), (130,–50), (80,–50), (80,–105), (80,70), (80,105), (–10,50), (–10,105), and (–10,–50). The data sample rate was 2 kHz with 12 bits of precision using the laptop-based data acquisition system. The data must be Fourier filtered into the appropriate frequency band from which the speeds may be derived. Data from impacts at these locations should be adequate to derive speeds throughout the entire empty booster shell. A preliminary analysis showed curvature in the speed when the unfiltered data are used.
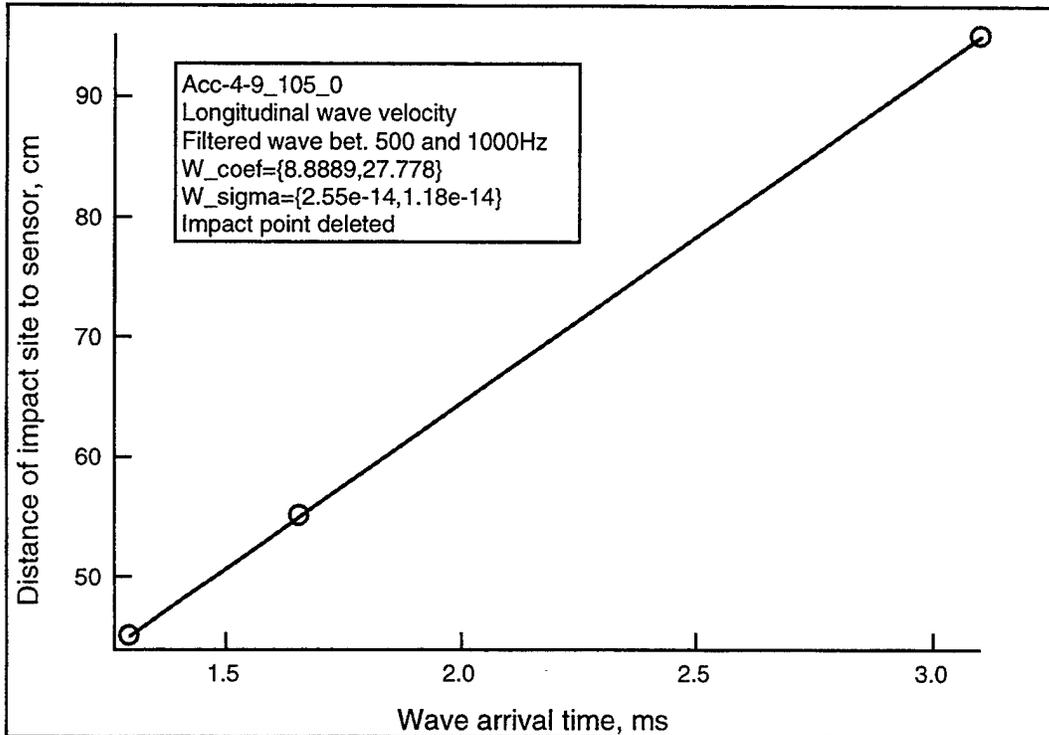
Figure 1.   Typical arrival times of impact at sensors in the longitudinal direction for a single impact
            point at (105, 0).
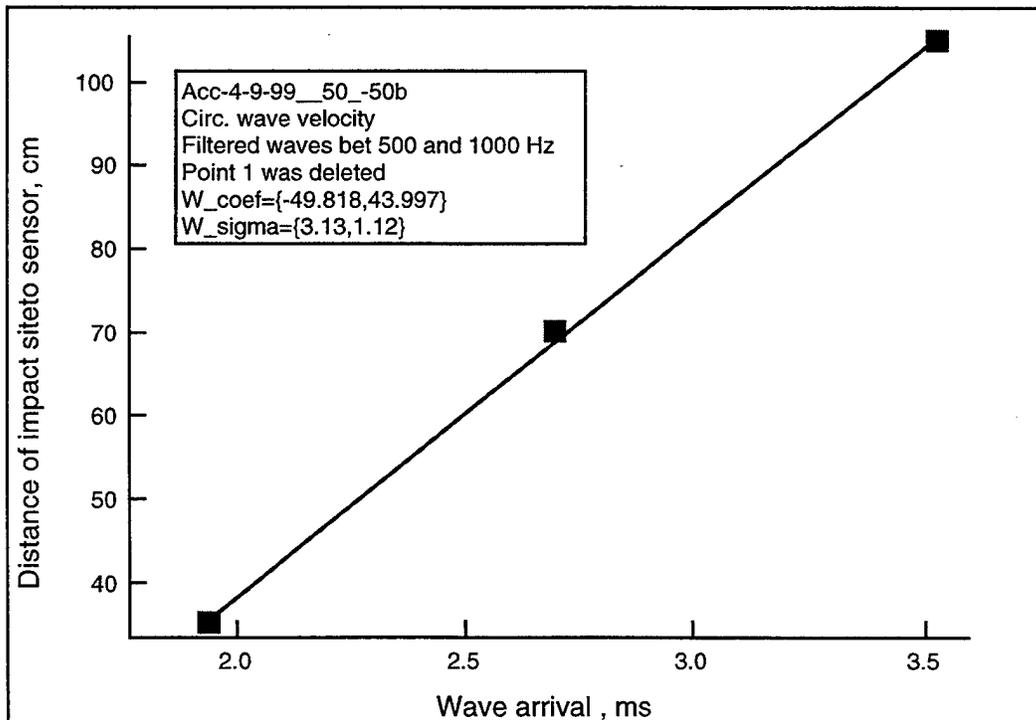
Figure2.   Typical arrival times of impact at sensors in the circumferential direction for a single
           impact point at (50,-50).

Table 1. Sensor Locations for Impacts with Rubber Hammer

Sensor ID	Sensor-Channel number	Location*(longitudinal) (cm)	Location* (from top, circumferential) (cm)
1	2 axis, longitude	0	0
2	2 axis, circumferential	0	0
3	2 axis longitude	200	0
4	2 axis, circumferential	200	0
5	1 axis longitude	175	-70
6	1 axis longitude	50	70
7	1 axis longitude	130	40
	Rubber mallet	various	various

*The coordinate system is the same as defined in section 2.

For the solid rocket motor case filled with an inert propellant, the situation was different. The inert propellant is a highly viscoelastic material. The material has many ingredients, including HTPB, NaCl (20 to 200 μm size particles), and aluminum particles (200 mesh). They generate high internal friction during deformation and thus have very high damping. The waves damped very rapidly at only a short distance away from the impact point. Therefore, the 50-g accelerometers were not sufficiently sensitive to generate useful information. Separate measurements with more sensitive accelerometers would be needed.

Since the inert-propellant-filled motor case would have a significantly different structural frequency response from the unfilled case, the wave speeds for the two motor cases would be different. The establishment of the wave speed for the filled case is necessary. The technique would be similar to what was described for the unfilled case.

4. Triangulation for Impact Location

The determination of the impact location during the monitoring of a solid rocket motor case has much utility. This approach should be applicable to all types of sensing devices, such as strain gages, accelerometers, and fiber optics. This section describes the mathematical derivation necessary to determine the impact location using the wave arrival time of three sensors at three distinct locations.

Since the motor case is made of high-modulus graphite fibers with epoxy as a resin, its mechanical properties are, in general, anisotropic. The symmetric fiber lay-up with respect to both longitudinal and circumferential directions makes its elastic properties orthotropic in the two-dimensional sense since the thickness of the composite is much less than either the longitudinal or circumferential dimension.

The surface of the motor case is treated as a two-dimensional plane with longitudinal and circumferential directions as the principal directions. Let the longitudinal direction be designated as the X direction, and the circumferential direction be designated as the Y direction in a rectangular coordinate system. The origin (0,0) is arbitrary. In the derivation, the following symbols are used:

α: X coordinate of the impact location

β: Y coordinate of the impact location

X_1:   X coordinate of sensor No. 1

X_2:   X coordinate of sensor No. 2

X_3:   X coordinate of sensor No. 3

Y_1:   Y coordinate of sensor No. 1

Y_2:   Y coordinate of sensor No. 2

Y_3:   Y coordinate of sensor No. 3

t_1:   wave travel time to sensor location 1

t_2:   wave travel time to sensor location 2

t_3:   wave travel time to sensor location 3

V_x: Wave speed in X direction (known)

V_y: Wave speed in Y direction (known)

λ: Ratio of V_y to V_x (V_y/V_x) (known)

The relation describing the contour of the wave front at time t_i is

$$\sqrt{[(X_i - \alpha)/V_x]^2 + [(Y_i - \beta)/V_y]^2} = t_i \quad i = 1,2,3 \tag{2}$$

The values of t_i are not known with regard to the time of impact, but the differences, $(t_2 - t_1)$ and $(t_3 - t_1)$, are measured for the purpose of locating the impact. Therefore, the three equations represented by Eq (2) can be rearranged to

$$\tag{3}$$

$$\sqrt{[(X_i - \alpha)]^2 + [(Y_i - \beta)/\lambda]^2} - \sqrt{[(X_1 - \alpha)]^2 + [(Y_1 - \beta)/\lambda]^2} = V_x(t_i - t_1) \quad i = 2,3$$

For convenience, let's designate

$$d_i = \left\{[(X_i - \alpha)]^2 + [(Y_i - \beta)/\lambda]^2\right\}^{1/2}, \quad I = 1,2,3$$

The two equations represented by Eq (3) can be used to solve for two unknowns, α and β. Since these two equations are nonlinear, and a closed-form solution is not obvious, an iterative approach needs to be taken. We will estimate the initial values of (α, β) as (α_0, β_0).

Let's designate functions f_2 and f_3 to represent the expressions on the left-hand side of Eq (3) with the index i equal to 2 and 3, respectively. The Taylor's expansions of f_2 and f_3 in the vicinity of (α, β) gives,

$$f_i(\alpha + \Delta\alpha, \beta + \Delta\beta) = f_i(\alpha,\beta) + f_{i,\alpha}\Delta\alpha + f_{i,\beta}\Delta\beta, \tag{4}$$

where $f_{i,\alpha}$ and $f_{i,\beta}$ are partial derivatives of f_i with respect to α and β, respectively, and $\Delta\alpha$ and $\Delta\beta$ are $(\alpha - \alpha_0)$ and $(\beta - \beta_0)$, respectively.

Explicitly, $f_{i,\alpha}$ and $f_{i,\beta}$ are written as follows:

$$f_{2,\alpha} = -(d_2)^{-1/2}(X_2 - \alpha) + (d_1)^{-1/2}(X_1 - \alpha) \tag{5}$$

$$f_{3,\alpha} = -(d_3)^{-1/2}(X_3 - \alpha) + (d_1)^{-1/2}(X_1 - \alpha)$$

$$f_{2,\beta} = [-(d_2)^{-1/2}(Y_2 - \beta) + (d_1)^{-1/2}(Y_1 - \beta)]/\lambda^2$$

$$f_{3,\beta} = [-(d_3)^{-1/2}(Y_3 - \beta) + (d_1)^{-1/2}(Y_1 - \beta)]/\lambda^2$$

A combination of Eqs (4) and (5) and the use of α_0 and β_0 leads to a linear matrix equation

$$\begin{bmatrix} f_{2,\alpha} & f_{2,\beta} \\ f_{3,\alpha} & f_{3,\beta} \end{bmatrix} \begin{pmatrix} \Delta\alpha_1 \\ \Delta\beta_1 \end{pmatrix} = -\begin{pmatrix} f_2(\alpha_0,\beta_0) \\ f_3(\alpha_0,\beta_0) \end{pmatrix} \tag{6}$$

This allows the determination of $\Delta\alpha_1$ and $\Delta\beta_1$, which are used to correct the initial estimate α_o and β_o. After the correction, one replaces the respective values of α_o and β_o with:

$$\alpha_1 = \alpha_o + \Delta\alpha_1$$
$$\beta_1 = \beta_o + \Delta\beta_1 \tag{7}$$

The values of α_1 and β_1 are then used as the new values of α and β in an iterative process using Eqs (5), (6), and (7). The recurrence formula for the iterative process is expressed as

$$\alpha_i = \alpha_{I-1} + \Delta\alpha_i$$
$$\beta_i = \beta_{i-1} + \Delta\beta_i \tag{8}$$

The iteration continues until a convergence is reached with a specified convergence criterion.

The above-described procedure was coded into an Excel file, and some test cases were examined. In general, convergence is reached in five to six iterations when the input warrants a solution. Otherwise, divergence will occur. One example of convergence is shown in Figure 3. As can be seen, the convergence occurs in four iterations despite the starting estimate of the impact origin (0,0) being far away from the actual solution (50,0). A simple error analysis using 500-Hz filtered waveform data could be used to estimate the uncertainty in the triangulation. Assuming good signal-to-noise ratio, the effective bandwidth is 250 Hz due to the Nyquist criteria. Thus, for a 240 m/s speed, the uncertainty in position is about 1 m for the worst case. If we average over two measurements, the position uncertainty is about 0.7 m. This independent estimate is in reasonable agreement with the error in the converged solution of the iteration procedure.

For a system that has more than three sensors close to the potential impact location with good signal-to-noise ratios, various subsets of three-sensor groups can be taken to approximate corresponding impact locations. For example, if five sensors have recorded good signals, the $^5C_3 = 10$ three-sensor groups would give 10 possible estimates of impact locations.

A least-square fitting procedure can also be used to give the best estimate of the impact location. A least-square fit approach can be described as follows. Assume there are N (N>3) data (sensor) points.

Define

$$\Delta_i = (\sqrt{d_i} - \sqrt{d_1}) - V_x(t_i - t_1) \qquad i = 2...N$$
$$\Delta^2 = \sum_{i=2}^{N} \Delta_i^2$$

Iterative procedure for approximate the impact origin								

Three sensors are used   Impact at (50,0)

Wave velocity Vx =   24035 cm/sec

Wave velocity Vy=   34180 cm/sec

Velocity ratio lamda=   1.422092781

Sensor 1   x1=   −40 cm
           y1   0 cm

Sensor 2   x2   50 cm
           y2   70 cm

Sensor 3   x3   100 cm
           y3   -64 cm

trial values   alpha=   0
                       beta=   0

Measured data   t2-t1=   -1.70E-03
                       t3-t1=   -9.00E-04

alpha	beta	f1,1st term	f1,2nd term	f1,3rd term	f1	f2	delta alpha	delta beta
0	0.00E+00	70.16356866	-40	40.8595	71.023	91.292	45.590218	-14.3024
45.59022	-1.43E+01	59.44429247	-86.179082	40.8595	14.125	0.1185	4.0513025	15.82807
49.64152	1.53E+00	48.15170758	-89.64794	40.8595	-0.637	0.2409	-0.073543	-0.7907
49.56798	7.35E-01	48.70829771	-89.569468	40.8595	-0.002	-2E-04	-0.000526	-0.00161
49.56745	7.33E-01	48.70943571	-89.568936	40.8595	-4E-09	3E-09	1.875E-10	-6.5E-09
49.56745	7.33E-01	48.70943571	-89.568936	40.8595	0	0	0	0
49.56745	7.33E-01	48.70943571	-89.568936	40.8595	0	0	0	0
49.56745	7.33E-01	48.70943571	-89.568936	40.8595	0	0	0	0

Figure 3. Illustrative example for triangulating impact location using three sensors.

Using the least-square approach with α and β as unknowns, one has

$$\Delta \frac{\partial \Delta}{\partial \alpha} = \sum_{i=2}^{N} [(\sqrt{d_i} - \sqrt{d_1}) - V_x(t_i - t_1)][\frac{(x_i - \alpha)}{\sqrt{d_i}} - \frac{(x_1 - \alpha)}{\sqrt{d_1}}] = 0$$

$$\Delta \frac{\partial \Delta}{\partial \beta} = \sum_{i=2}^{N} [(\sqrt{d_i} - \sqrt{d_1}) - V_x(t_i - t_1)][\frac{(y_i - \beta)}{\sqrt{d_i}} - \frac{(y_1 - \beta)}{\sqrt{d_1}}]/\lambda^2 = 0$$

or   (8)

$$\sum_{i=2}^{N} (\sqrt{d_i} - \sqrt{d_1})[\frac{(x_i - \alpha)}{\sqrt{d_i}} - \frac{(x_1 - \alpha)}{\sqrt{d_1}}] = \sum_{i=2}^{N} V_x(t_i - t_1)[\frac{(x_i - \alpha)}{\sqrt{d_i}} - \frac{(x_1 - \alpha)}{\sqrt{d_1}}]$$

$$\sum_{i=2}^{N} (\sqrt{d_i} - \sqrt{d_1})[\frac{(y_i - \beta)}{\sqrt{d_i}} - \frac{(y_1 - \beta)}{\sqrt{d_1}}]/\lambda^2 = \sum_{i=2}^{N} V_x(t_i - t_1)[\frac{(y_i - \beta)}{\sqrt{d_i}} - \frac{(y_1 - \beta)}{\sqrt{d_1}}]/\lambda^2$$

12

The values of α and β can be solved iteratively in a way similar to that described for Eqs (4) through (7) in the three-sensor case. Conversely, a general two-dimensional fitting procedure may be used as implemented in the IGOR software package from Wavemetrics.

This least-squares approach was not tested due to time constraints, but is considered to be a sound approach. Prior to its consideration, a simpler, cruder test of the elliptical speed profile was considered. Unfiltered data was used to derive the longitudinal and circumferential speeds, and the expected arrival times at sensors were plotted against the measured arrival times, again unfiltered. In general a 1–2 ms error was observed, which translates into approximately a 0.8-m error. With a least-square fit, a more self-consistent speed, and well-defined arrival times at the sensors, the error in localization of the impact site is expected to improve significantly.

5. Road Tests of GPS Position Location

In addition to the accelerometer measurements, GPS position information was recorded during road tests with the inert motor. The instrumentation consisted of a GPS receiver with data logging software on a laptop. General information includes position as a function of time, the number of satellites seen by the receiver, velocity, etc. Since GPS time is very accurate, it is simple and convenient to synchronize observed events to it from the laptop display. Events were noted on a log book with regard to a wrist watch and the offset time was noted to the GPS clock time. The log book events could then be corrected for the offset.

Accuracy for civilian non-differential GPS is limited to 100 m. The GPS receiver was situated on the top of the driver cab of the GEM transport vehicle, the highest point of the combined tractor-flatbed-inert booster configuration. Location readings were logged at the rate of one per second. Observations of time of events and landmarks were made from a chase car and time-correlated to GPS position information.

The GPS data and the logged observations listed in Tables 2 through 4 can be used to correlate acceleration or strain events with particular locations or road hazards experienced via time correlations. Its use is discussed by Amimoto.[5]

The hangar that houses the GEM under study is located at 117° 41.07′ West longitude, 34° 55.89′ North latitude. A list of recorded data is shown in Table 2. Examples of road tests are shown in Tables 3 and 4. The corresponding track mapping for the 3-mile route related to Table 4 is shown in Figure 4.

Table 2. List of GPS Data Files Recorded During Road Tests

File	Start Time	End Time	Description
GPS1	14:06:16	14:06:49	Stationary at hangar
GPS2	14:07:06	14:17:22	Drive around hangar, 1 loop
GPS3	14:17:40	14:24:53	Drive around hangar, 2 loops
GPS4	14:25:07	14:34:10	Drive around hangar, 2 loops
GPS5	14:34:27	14:50:36	Small maneuvers at hangar
GPS6	14:50:38	15:09:54	Short drive on roads
GPS7	15:10:34	15:40:54	Three-mile drive to Propellant Storage Complex and back to hangar

15

Table 3.   Observations and Position Information During Road Tests Drive on
           Roads (File GPS6)

Comment	Time	117 W Lon (min)	34 N Lat (min)
Short Drive on roads begins	14:51:20	41.07	55.90
Driveway from hangar	14:53:30*	41.32	55.90
Strap Breaks	14:54:30*	41.33	55.92
Part 2 of drive starts moving	15:02:51	41.30	55.91
Left turn from Mercury	15:04:51	41.46	55.82
Right turn	15:05:10	41.47	55.78
Right turn	15:05:31	41.53	55.74
Right turn onto Mercury from Mars	15:05:48	41.58	55.75
Right turn	15:06:25	41.45	55.86
Left turn	15:06:59	41.22	55.87
Right turn	15:07:06	41.19	55.89
Dirt road	15:07:23	41.12	55.90
Right turn	15:07:38	41.07	55.90
Stop, back at hangar	15:07:48	41.07	55.89

Table 4.   Three-mile drive from hangar to Propellant Storage Complex and back
           to hangar (File GPS7)

Comment	Time	117 W Lon (min)	34 N Lat (min)
Begin	15:13:51	41.07	55.88
Indus and Persea on Antares Road	15:15:25	41.18	55.87
Left turn	15:16:00*	41.46	55.83
Left onto Mars from Mercury, bump	15:16:56	41.59	55.74
Bump	15:18:06	41.38	55.44
Travelling at 20 mph	15:18:37	41.26	55.33
Continuing on straight road	15:21:07	40.61	54.76
Left turn	15:23:23	40.03	54.24
Right turn	15:23:43	39.99	54.26
Stop at Propellant Storage Complex	15:23:59	39.97	54.25
Back onto pavement	15:30:16	39.99	54.24
Travelling at 40 mph, straight road	15:31:01	39.98	54.22
Travelling at 35 mph, straight road	15:33:43	40.92	55.04
Road curves to right	15:34:53	41.39	55.47
Passed over 2 bumps	15:35:38	41.56	55.71
Right turn on Mercury from Mars	15:35:51	41.58	55.74
Right turn on Antares	15:36:27	41.44	55.87
Left on Indus	15:37:02	41.21	55.88
Right turn	15:37:09	41.18	55.89
On dirt at driveway to hangar	15:37:21	41.12	55.90
Stopped	15:37:45	41.09	55.90
Backing into hangar	15:38:36	41.10	55.92

*Estimated

16

Three Mile Drive to Propellant Storage Complex and Return to Hangar
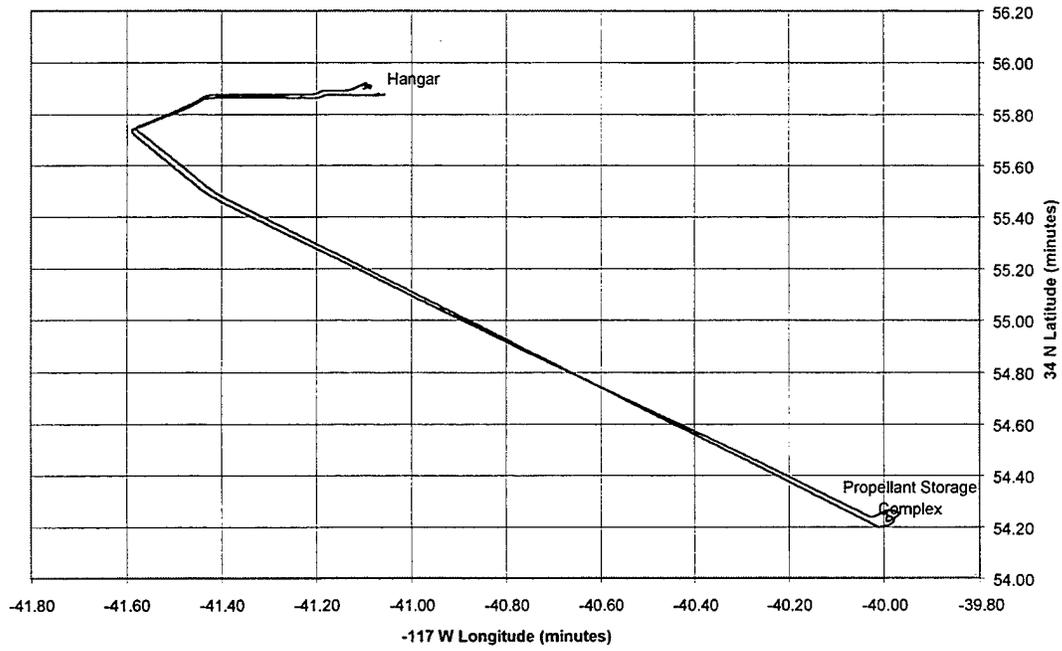

Figure 4. Position track from File GPS7.

6. Lessons Learned

- Sufficient preparation time is needed to prepare instrumentation and test procedures. Dry runs are invaluable to meeting test schedules, and ensuring successful equipment operation and reliable data collection.

- Predicting the acceleration amplitudes is difficult for the field tests. It seems that sensitivities of 1–5 g are needed for the filled GEM, but the values should also be based on performance requirements of the components to be tested.

- Several test opportunities are needed not only to test out equipment but to also understand configuration and validate test procedures.

- Additional effort is needed to quantify the impact-induced wave speeds and how well localization of impact site can be achieved.

7. Conclusions

We have identified an approach to the measurement of wave speeds in composite solid rocket motor cases. Frequency filtering must be used on the observed waveforms to derive consistent values of wave speed to overcome the dispersion effects predicted by the Kirchoff equation. Some care must be taken to examine the frequency content of impacts in order to select an adequate frequency range for the speed measurement. For free-fall impacts, variations in the mass of the impacting object, the softness of its impacting face, and the stiffness of the object under impact will generate waves with various frequency ranges and thus will produce inconsistent wave speeds. These speeds can be used in an elliptical model with a least-square approach to localize the origin of the impact. These wave speeds are associated with structural deformations and not the prompt, longitudinal wave component associated with the modulus of the fiber. This work then validates the assumptions that enables one to find the impact location on the composite booster. More sensitive accelerometers, 1 to 5 g, must be used to overcome the damping that is observed when the inert propellant is present. Lastly, the use of GPS position recordings has high value to correlate position with acceleration or other events of note.

References

1. K. Olofsson, K. E. Fallstrom, and P. Palagyi, "Laser generated and recorded transient bending waves in composite tubes," 36, pp 224-231, 1996.

2. E. Fallstrom, H. Gustavsson, N. E. Molin, and A. Wahlin, "Transient Bending Waves in Plates Studies by Holographic Interferometry", *Experimental Mechanics*, 29 (4), pp 409-413, 1989.

3. K. E. Fallstrom, L. E. Lindgren, N. E. Molin, and A. Wahlin, *Experimental Mechanics*, 29 (4), pp 378-408, 1989.

4. S. Urgela, "Grading of wooden plates for musical instrument making by means of holographic interferometery," Opt. Eng., 37, pp 2108-2117, 1998.

5. S. T. Amimoto, R. Crespo, E. W. Fournier, M. A. Kwok, H. Ozisik, R. Y. Robinson, and E. M. Yohnsee, "Atlas Payload transporter vibration and acceleration characterization using MEMS sensors at Vandenberg AFB", Aerospace Report, no. TOR-98(8260)-1.

TECHNOLOGY OPERATIONS

The Aerospace Corporation functions as an "architect-engineer" for national security programs, specializing in advanced military space systems. The Corporation's Technology Operations supports the effective and timely development and operation of national security systems through scientific research and the application of advanced technology. Vital to the success of the Corporation is the technical staff's wide-ranging expertise and its ability to stay abreast of new technological developments and program support issues associated with rapidly evolving space systems. Contributing capabilities are provided by these individual organizations:

Electronics Technology Center: Microelectronics, VLSI reliability, failure analysis, solid-state device physics, compound semiconductors, radiation effects, infrared and CCD detector devices, data storage and display technologies; lasers and electro-optics, solid state laser design, micro-optics, optical communications, and fiber optic sensors; atomic frequency standards, applied laser spectroscopy, laser chemistry, atmospheric propagation and beam control, LIDAR/LADAR remote sensing; solar cell and array testing and evaluation, battery electrochemistry, battery testing and evaluation.

Mechanics and Materials Technology Center: Evaluation and characterizations of new materials and processing techniques: metals, alloys, ceramics, polymers, thin films, and composites; development of advanced deposition processes; nondestructive evaluation, component failure analysis and reliability; structural mechanics, fracture mechanics, and stress corrosion; analysis and evaluation of materials at cryogenic and elevated temperatures; launch vehicle fluid mechanics, heat transfer and flight dynamics; aerothermodynamics; chemical and electric propulsion; environmental chemistry; combustion processes; space environment effects on materials, hardening and vulnerability assessment; contamination, thermal and structural control; lubrication and surface phenomena.

Space and Environment Technology Center: Magnetospheric, auroral and cosmic ray physics, wave-particle interactions, magnetospheric plasma waves; atmospheric and ionospheric physics, density and composition of the upper atmosphere, remote sensing using atmospheric radiation; solar physics, infrared astronomy, infrared signature analysis; infrared surveillance, imaging, remote sensing, and hyperspectral imaging; effects of solar activity, magnetic storms and nuclear explosions on the Earth's atmosphere, ionosphere and magnetosphere; effects of electromagnetic and particulate radiations on space systems; space instrumentation, design fabrication and test; environmental chemistry, trace detection; atmospheric chemical reactions, atmospheric optics, light scattering, state-specific chemical reactions and radiative signatures of missile plumes.

Center for Microtechnology: Microelectromechanical systems (MEMS) for space applications; assessment of microtechnology space applications; laser micromachining; laser-surface physical and chemical interactions; micropropulsion; micro- and nanosatellite mission analysis; intelligent microinstruments for monitoring space and launch system environments.

Office of Spectral Applications: Multispectral and hyperspectral sensor development; data analysis and algorithm development; applications of multispectral and hyperspectral imagery to defense, civil space, commercial, and environmental missions.